

FIG. 4. Regressions of shell mass (A) and egg number (B) against body length for the conic (●) and bent (○) morphs of *Chthamalus anisopoma*. The vertical axes were back-transformed from $\log(x)$.

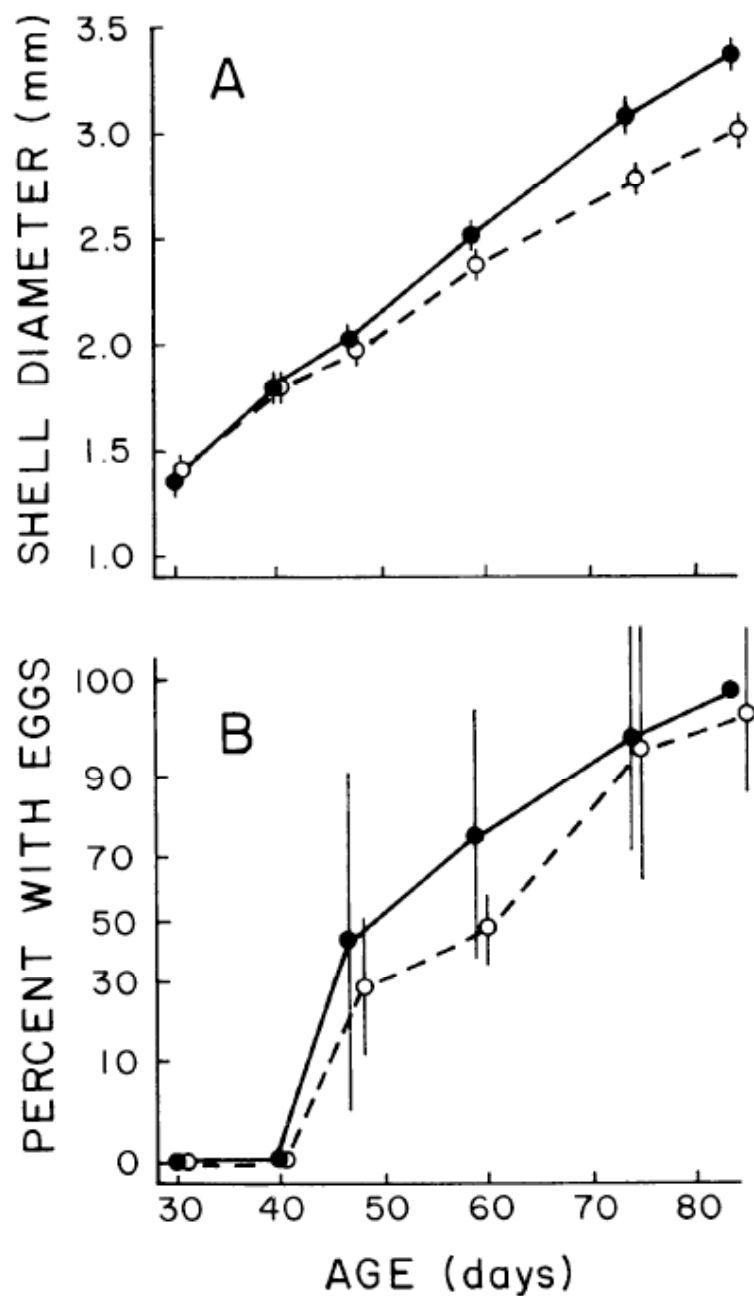


FIG. 3. Shell (rostro-carinal) diameter (A) and percent of individuals with eggs (B) as a function of age for the conic (●) and bent (○) morphs of *Chthamalus anisopoma*. Vertical bars are 95% confidence intervals of the means. Percentages were back-transformed from arcsine \sqrt{P} .

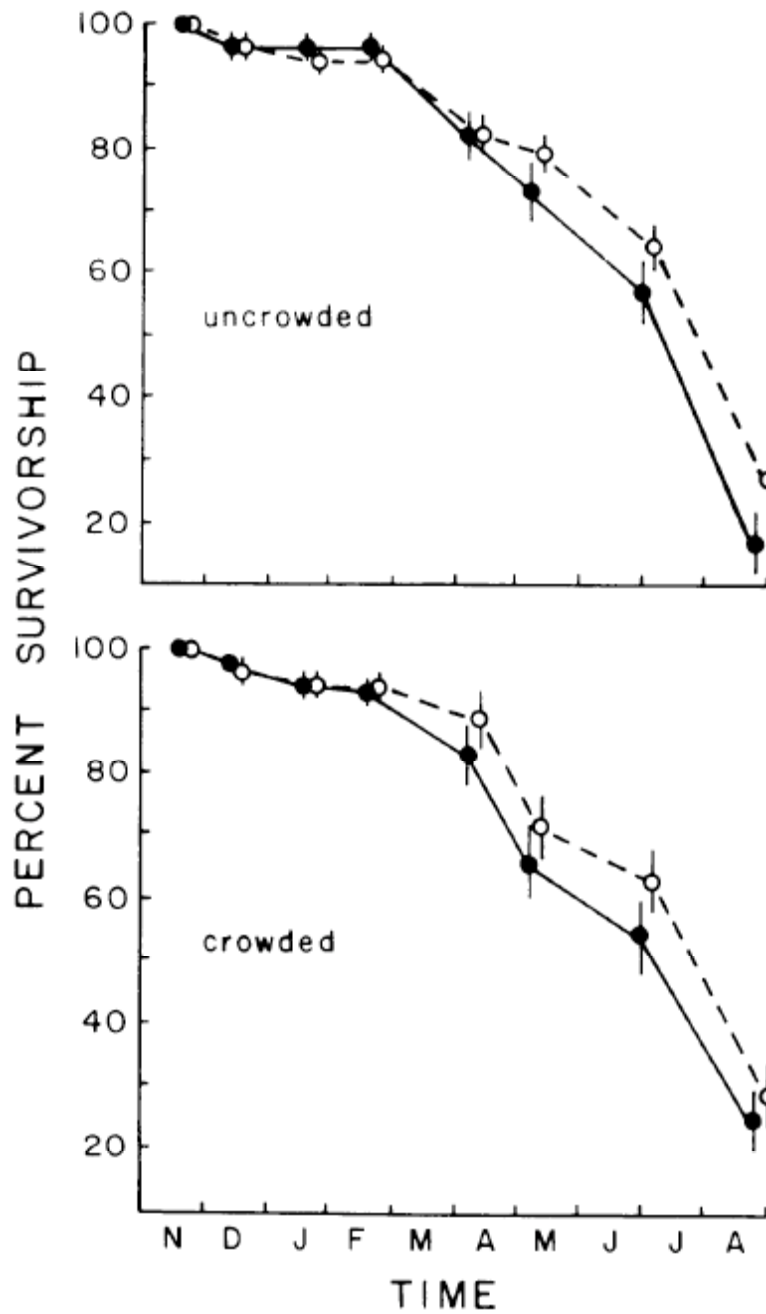


FIG. 2. Survivorships over time for the conic (●) and bent (○) morphs of *Chthamalus anisopoma* under crowded and uncrowded conditions in the competition experiment. Vertical bars are ± 1 standard error about the mean.

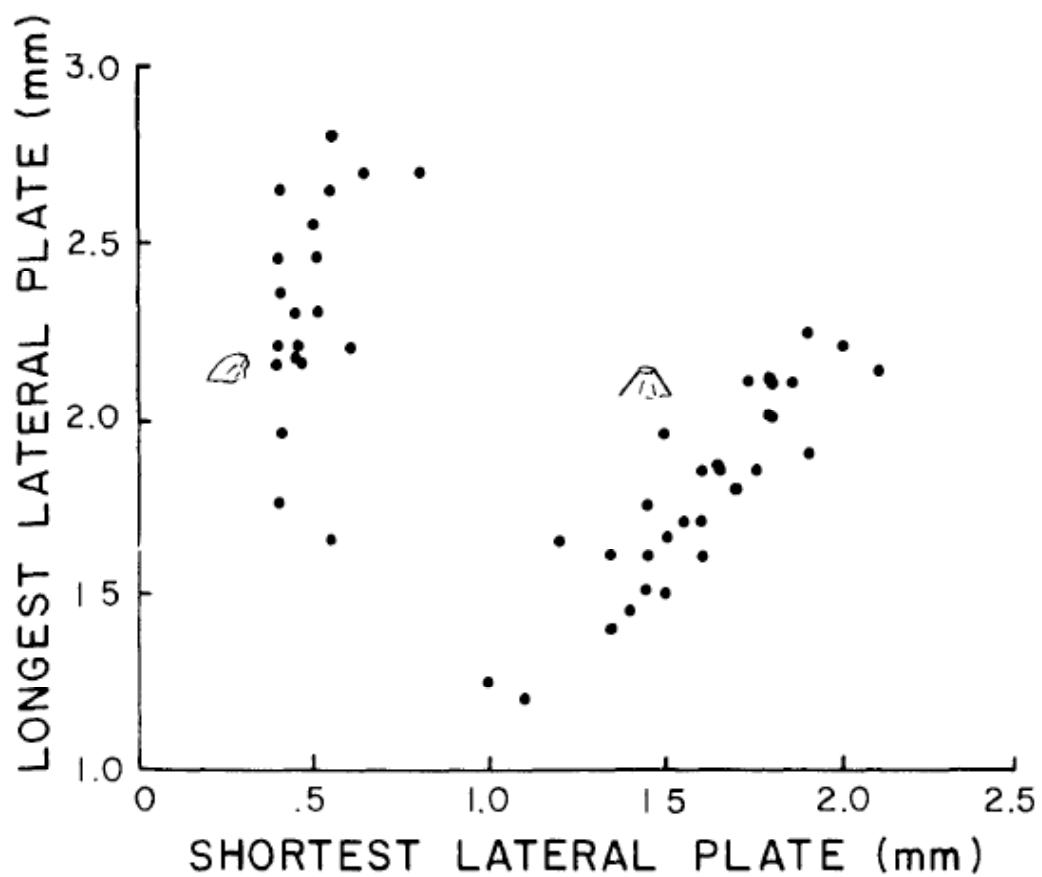


FIG. 2. A bivariate plot of the lengths of the shortest against the lengths of the longest lateral plates for 50 *C. anisopoma*.

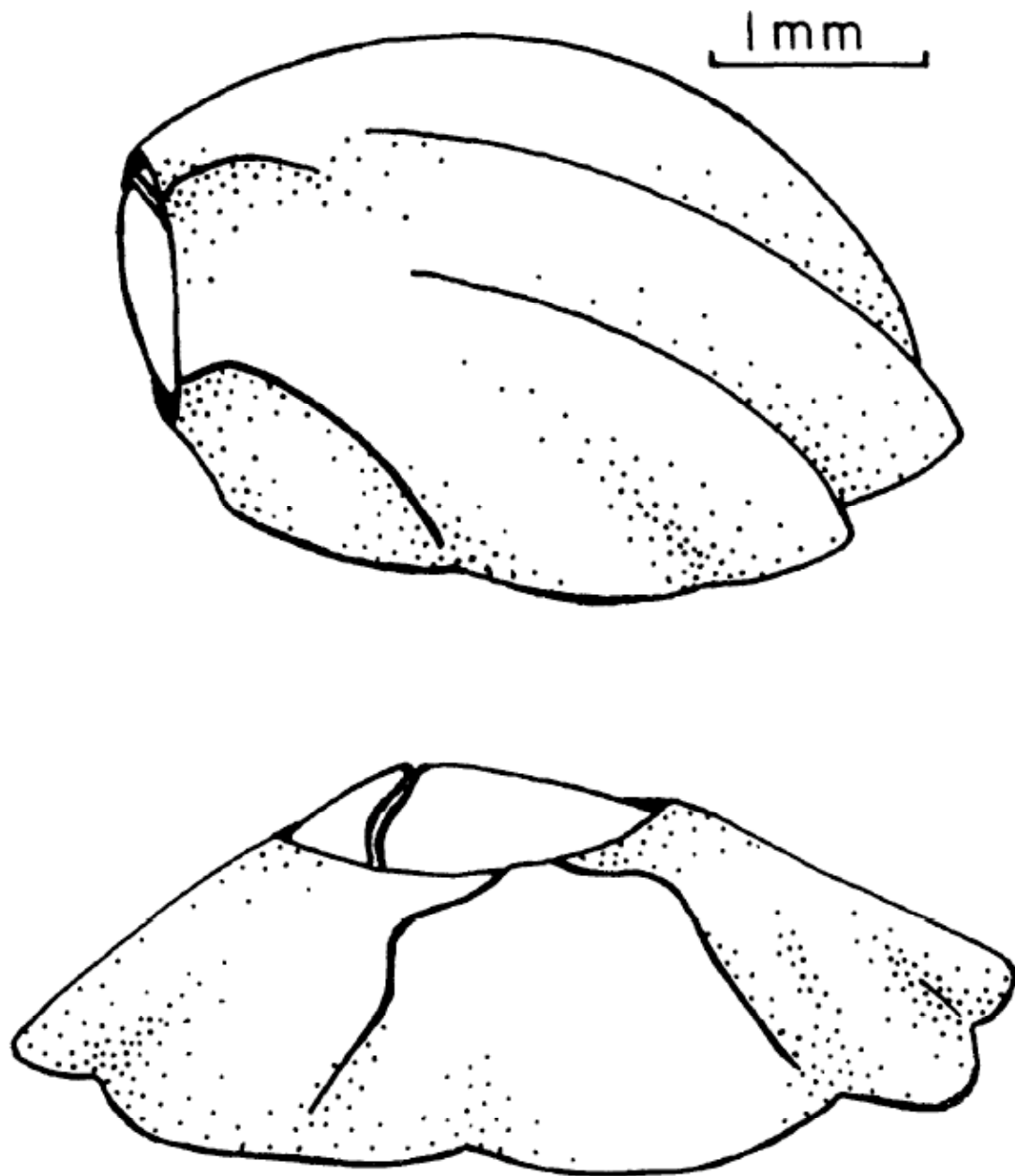


FIG. 1. Line drawings of the bent (top) and conic morphs of *C. anisopoma*. The rostro-carinal axis of the bent morph is drawn as perpendicular to both the plane of the page and that shown for the conic morph. The apertures of both morphs are closed by the opercular valves (scutum and tergum) of one side only. The right and left valves are generally asymmetric with respect to size (Pilsbry, 1916)

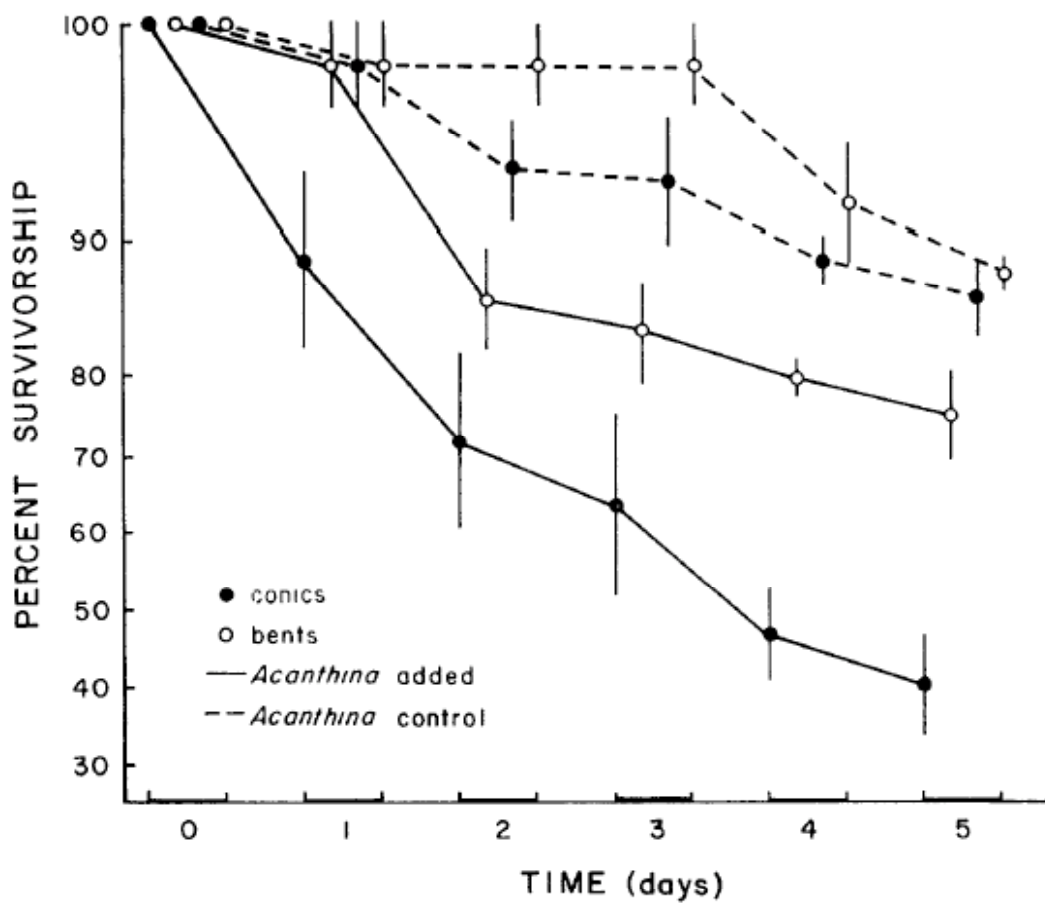


FIG. 3. Survivorship by bent and conic morphs of *C. anisopoma* in the *A. angelica* predation experiment. Percentages were back-transformed from arcsine \sqrt{p} . Vertical bars are one standard error of the mean.